Journal of Qassim University for Science
2025, *Vol 4* (Issue 1), pp. 156-182.

Received: 8 September 2024
Revised: 5 October 20234
Accepted: 20 October 2024
Published: 27 April 2025

JQUS

Thermal Properties of ^{4}He, ^{16}O and ^{40}Ca Isotopes Using Harmonic Oscillator Nuclear Potential

Hajar Al-Hatlani, Abeer Al-Nasser, and Bassam Shehadeh
Physics Department, College of Science,
Qassim University, Qassim, Burydah 51411, KSA.

(Date textdate; Received textdate; Revised textdate; Accepted textdate; Published textdate)

Abstract

In this study, we examine the thermal properties of ^{16}O and ^{40}Ca isotopes utilizing an independent quasi-particle model within a three-dimensional harmonic oscillator potential as the mean-field potential. Our calculations are grounded in quantum statistics within the canonical ensemble framework, from which we derive the partition function. We construct the partition functions using two distinct models: the first treats nucleons as a fermion gas and employs an antisymmetric partition function recursion formula incorporating bulk spin pairings based on Hund's rule. The second model considers the nucleon system as isoscalar clusters of spin vector bosons. Subsequently, we compute the thermal energy and heat capacity as functions of temperature. Furthermore, we calculate the level density and compare it with available experimental data. The results are promising, displaying excellent agreement with the experimental level densities.

PACS numbers: 21.10.Ma, 21.10.Pc, 21.60.Cs, 21.60.n, 24.10.Cn, 24.10.Pa

Keywords: Nuclear physics, Statistical spectroscopy, Thermal properties of nuclei, level densities.

I. INTRODUCTION

In nuclear scattering processes, such as inelastic heavy ion scattering and fusion reactions, energy is transferred from the relative motion of the colliding nuclei to the internal degrees of freedom of the reaction products. This transformation of energy may be an efficient method of heating nuclei. Knowing the thermal properties for nuclear systems is of great importance for understanding these reaction processes.

Nuclei under such conditions often exhibit behaviors akin to liquid drops, capable of undergoing phase transitions that can be described by models considering the van der Waals-like interactions of the nuclear force. Such models predict liquid-gas phase transitions in nuclei, supported by experimental evidence observed in fragmentation patterns produced in proton-induced nuclear collisions [1].

This study utilizes the three-dimensional Harmonic Oscillator (3DSHO) model to investigate the thermal properties of ^{4}He, ^{16}O and ^{40}Ca isotopes. This model simplifies the complex interactions within nuclei and provides a clear framework for understanding their thermal behavior at various excitation energies. The canonical ensemble approach, used to model the system in thermal equilibrium, allows for detailed analysis of the single-particle (SP) energy levels and their population under thermal stress, thus influencing the nuclear stability against deformation [2].

The focus on ^{4}He, ^{16}O and ^{40}Ca, all of which are stable and doubly magic isotopes, is due to their closed shell characteristics, which simplify many-body interactions and make them ideal subjects for theoretical studies. By comparing the calculated thermal properties, such as excitation energy, heat capacity, and level density, with experimental data, we aim to calibrate the validity of our model and the approximations used to account for pairing effects.

II. THE SYSTEM HAMILTONIANS

In this section, we present the Hamiltonian used in the applications of later sections. We choose the three-dimension simple harmonic oscillator (3DSHO) as the mean-field potential for modeling the nuclear matter of ^{4}He, ^{16}O and ^{40}Ca Isotopes.

A. The Three-Dimensional Harmonic Oscillator

The 3DSHO serves as a simple qualitative guide for the statistical properties of nuclei at moderate excitation energies or temperatures where details of the NN interactions and intrashell SP details are less important. For a doubly magic nuclei like ^{4}He, ^{40}Ca and ^{16}O, the 3DSHO may be somewhat more useful as its non-degenrate ground state and large gap more closely resemble physical reality than the case of open shell nuclei.

Hamiltonian and Energy Levels

In a given many body state, N identical non-interacting particles in the 3DSHO occupy SP states labelled by i = 1,2,..., N, each with its SP energy

$$\varepsilon^i = \left(n_x^i + n_y^i + n_z^i + \frac{3}{2}\right)\hbar\omega. \tag{1}$$

The total energy for that state can be defined, in terms of an integer j, as

$$E_j = \sum_i^N \varepsilon^i = (\underbrace{\sum_i^N n_x^i + n_y^i + n_z^i}_{j} + \frac{3N}{2})\hbar\omega = \left(j + \frac{3N}{2}\right)\hbar\omega.$$

Canonical Partition Function

Performing this sum for the lowest 3DSHO configuration corresponding to ^{4}He, ^{16}O and ^{40}Ca leads to 3DSHO ground states with energies $(6\hbar\omega)$,$(24\hbar\omega)$ and $(120\hbar\omega)$. From quantum statistics, the canonical partition function for N particles are given as

$$\mathcal{Z}_N = \sum_{j=0}^{\infty} g_j \exp\left[-\beta\left(j + \frac{3N}{2}\right)\hbar\omega\right], \tag{2}$$

where g_j is the degeneracy of the j^{th} state and $\beta = (k_B T)^{-1}$. For N particles in the 3DSHO, the factor g_j is not known in closed form for both fermion and bosons [3]. It is sufficient for our purposes to obtain a closed form for the single-particle (SP) partition function in the 3DSHO which is given by

$$\mathcal{Z}_1(\beta) = \left(\frac{\exp\left(-\frac{\beta\hbar\omega}{2}\right)}{1 - \exp\left(-\beta\hbar\omega\right)}\right)^3. \tag{3}$$

This SP partition function is the starting point to obtain information about the many-fermion system in the 3DSHO as will be shown in Section (III)

III. STATISTICAL MECHANICS IMPLEMENTATION

A. Introduction

In this section we utilize the population of single-particle (SP) states thermally by nucleons using the canonical ensemble and we account for additional interaction effects. The thermal population of the single-particle (SP) states can be carried out for the desired number of nucleons using the antisymmetric summation of fermionic partition functions for subsystems through the recursion relation given in Ref. [4]. For n identical particles subject to any SP Hamiltonian (i.e. omitting particle-particle interactions), the canonical partition function can be constructed starting with the SP partition function [4]

$$\mathcal{Z}_n^{\pm}(\beta) = \frac{1}{n}\sum_{i=1}^{n} (\pm 1)^{i+1} \mathcal{Z}_1(i\beta)\mathcal{Z}_{n-i}^{\pm}(\beta), \qquad \mathcal{Z}_0(\beta) = 1, \tag{4}$$

where the plus and the minus signs stand for bosons and fermions, respectively. The recursion formula (4) gives exact values of the partition functions at specific values of n [4]. Earlier implementations of similar recursion formulas were carried out to obtain observables for nuclear systems $[5 - 8]$.

In the 3DSHO when $n = 1, \mathcal{Z}_1^{\pm}(\beta) = \mathcal{Z}_1(\beta)$ and the starting point to build the partition function is given by Eq.(3). The partition functions $\mathcal{Z}_n^{\pm}$are then rational functions of $y = \exp\,(-\hbar\omega)$ and can be expanded in a power series [9-11]

$$\mathcal{Z}_n^{\pm}(y) = \frac{y^{\frac{3n}{2}}}{\prod_{j=1}^{n}\,(1-y^j)^3} P_n^{\pm}(y), \tag{5}$$

where $P_n^{\pm}(y)$ is a polynomial in y. Substituting Eq.(5) into Eq.(4), we obtain a recursion relation for the polynomials:

$$P_n^{\pm}(y) = \frac{1}{n}\sum_{k=1}^{N} (\pm 1)^{k+1} \frac{\prod_{j=n-k+1}^{n}\,\left(1-y^j\right)^3}{(1-y^k)^3} P_{n-k}^{\pm}(y), \tag{6}$$

where $P_0^{\pm}(y) = P_1^{\pm}(y) = 1$ [9]. Although the partition functions can be obtained using Eq.(4), the polynomials in Eq.(5) lead to improved stability in the numerical evaluation since they are better behaved near the boundaries of y. For larger numbers of particles, the evaluation of the partition function near zero temperature is very difficult. Therefore, we employ numerical techniques which factorize and test each term to avoid overflow or underflow. In addition, we implement a multi-precision algorithm called "quad double" developed by Hida and Bailey [12, 13] which enables us to compute observables up to 212 bits of floating-point accuracy.

B. Configuration-Restricted Recursion

We restrict the configurations when recursively constructing the partition function in order to take into account pairing effects. The technique is implemented for a fixed species of nucleon (protons or neutrons) by constructing the partition function for a subgroup of that species to represent a specific value of the magnetic projection of the total angular momentum quantum number.

Now let $A = Z + N$, where A, Z, and N are the mass, the atomic, and the neutron numbers, respectively. For ^{40}Ca, an even-even nucleus, we evaluate the partition function first for, say, spin-up protons and neutrons, $\mathcal{Z}_{Z/2}^{(\uparrow)}$ and $\mathcal{Z}_{N/2}^{(\uparrow)}$, respectively. Then we evaluate the partition function for spin-down protons and neutrons, $\mathcal{Z}_{Z/2}^{(\downarrow)}$ and $\mathcal{Z}_{N/2}^{(\downarrow)}$, respectively. The total nuclear partition function is thus

$$\mathcal{Z}_A(\beta) = \underbrace{\left(\mathcal{N}_Z \mathcal{Z}_{Z/2}^{(\uparrow)} \mathcal{Z}_{Z/2}^{(\downarrow)}\right)}_{\mathcal{Z}_Z^{(\uparrow\downarrow)}} \underbrace{\left(\mathcal{N}_N \mathcal{Z}_{N/2}^{(\uparrow)} \mathcal{Z}_{N/2}^{(\downarrow)}\right)}_{\mathcal{Z}_N^{(\uparrow\downarrow)}}, \tag{7}$$

where $\mathcal{N}_Z$ and $\mathcal{N}_N$ are proton and neutron normalization factors, given by

$$\mathcal{N}_i = \frac{\Omega_i^{(\uparrow\downarrow)}}{\Omega_{i/2}^{(\uparrow)} \Omega_{i/2}^{(\downarrow)}}; \quad \forall i = Z \text{ or } N, \tag{8}$$

where Ω is total number of accessible states.

Once the partition function is computed for the desired system at a given temperature, the observables, such as the average thermal energy E_A, the heat capacity C_A, and the level density g_A can be computed, respectively, in the canonical ensemble as

$$E_A(\beta) = -\frac{\partial}{\partial\beta}\log\,\mathcal{Z}_A(\beta); \qquad C_A(\beta) = -k_B\beta^2\frac{\partial E_A}{\partial\beta}, \tag{9}$$

and

$$g_A(E) = \frac{\beta e^{S(\beta)/k_B}}{\sqrt{2\pi C_A(\beta)/k_B}} = \frac{\beta}{\sqrt{2\pi C_A(\beta)/k_B}}\mathcal{Z}_A(\beta)e^{\beta E_A(\beta)}. \tag{10}$$

Eq.(10) is calculated using method of steepest descent [3]. The factor $\mathcal{Z}_A(\beta)\exp\,(\beta E_A(\beta))$ is the number of microstates $\Omega(E)$. We can easily prove in the canonical ensemble that [3]

$$\Delta E \equiv \sqrt{\langle E_A^2\rangle - \langle E_A\rangle^2} = \frac{1}{\beta}\sqrt{C_A(\beta)/k_B}\,. \tag{11}$$

Therefore Eq.(10) can be written as

$$g_A(E) = \frac{1}{\sqrt{2\pi}}\frac{\Omega(E)}{\Delta E}.$$

As $\beta \to \infty, \Delta E \to 0$, the canonical ensemble is not a valid approach to evaluate level densities only since statistics are low near zero temperatures. Here, the microcanonical ensemble could be used to obtain level densities.

To evaluate the nuclear thermal properties using the 3DSHO, we use Eqs.(7-10) together with Eqs.(4-6).

C. Symbolic Approach

For ^{4}He, ^{6}He, and ^{16}O we use Mathematica in computing the partition functions and the rest of observables up to level densities. We start from single particle oscillator in 1D

$$\varepsilon_n = -V_0 + \left(n + \frac{1}{2}\right)\hbar\omega. \tag{12}$$

The partition function for a single particle 1-D oscillator is:

$$Z_1^{1d}(\beta) = \sum_n e^{-\varepsilon_n \beta} = \sum_{n=0}^{\infty} e^{-\left[-V_0 + \left(n+\frac{1}{2}\right)\hbar\omega\right]\beta}$$
$$= \sum_{n=0}^{\infty} e^{V_0\beta} e^{-\hbar\omega\beta/2} e^{-n\hbar\omega\beta}$$
$$= e^{V_0\beta} e^{-\hbar\omega\beta/2} \sum_{n=0}^{\infty} \left(e^{-\hbar\omega\beta}\right)^n \tag{13}$$
$$= e^{V_0\beta} \frac{e^{-\hbar\omega\beta/2}}{1 - e^{-\hbar\omega\beta}}$$

For a in 3-D oscillator, the single particle partition becomes:

$$Z_1^{3d}(\beta) = \left(Z_1^{1d}(\beta)\right)^3 = e^{3V_0\beta} \left(\frac{e^{-\hbar\omega\beta/2}}{1 - e^{-\hbar\omega\beta}}\right)^3. \tag{14}$$

Using $x = e^{-\hbar\omega\beta}$, we can express the 3-D partition function as:

$$Z_1^{3d}(\beta) = x^{-\frac{3V_0}{\hbar\omega}} \left(\frac{x^{1/2}}{1 - x}\right)^3. \tag{15}$$

General Simplifications

For Fermions:

The generalized partition function is:

$$Z_A(x) = \frac{1}{\left(\frac{A}{4}!\right)^4} x^{A\left(\frac{3}{2} - 3\frac{V_0}{\hbar\omega}\right)} f_A(x) \tag{16}$$

Calculating the Potential depth from the ground state energy for fermions:

$$\left(E_{^4\mathrm{He}}^{\mathrm{F}}\right)_{gs} = 6\hbar\omega - 12V_0 \tag{17}$$

$$\left(E^{\mathrm{F}}_{6_{\mathrm{He}}}\right)_{gs} = 11\hbar\omega - 18V_0 \tag{18}$$

$$\left(E^{\mathrm{F}}_{16_O}\right)_{gs} = 36\hbar\omega - 48V_0 \tag{19}$$

$$\left(E^{\mathrm{F}}_{40_{Ca}}\right)_{gs} = 120\,\hbar\omega - 120V_0 \tag{20}$$

The potential depth for fermionic oscillators, calculated from the ground state energy which must equal the binding energy as follows:

$$(V_0)^F_{4_{He}} = \frac{\hbar\omega + 4.71594}{2} \tag{21}$$

$$(V_0)^F_{6_{He}} = \frac{11\hbar\omega + 29.271}{18} \tag{22}$$

$$(V_0)^F_{16_O} = \frac{3\,\hbar\omega + 10.635}{4} \tag{23}$$

$$(V_0)^F_{40_{Ca}} = \hbar\omega + 2.850435 \tag{24}$$

Note: For fermions, unlike bosons, we were not able to find a general formula for ground state energy similar to Eq. (26). This is likely due to the influence of the Pauli exclusion principle, which leads to a more complex filling of energy levels that varies significantly between different nuclei.

For Bosons

For N bosons the generalized partition function is:

$$Z^B_N(x) = \frac{1}{N!}x^{N\left(\frac{3}{2}-3\frac{V_0}{\hbar\omega}\right)}f_N(x) \tag{25}$$

The generalized ground state energy for bosons:

$$E^B_{gs} = N\left(\frac{3}{2}\hbar\omega - 3V_0\right) \tag{26}$$

Calculating the Potential depth from the ground state energy for Bosons:

$$\left(\mathrm{E}^{\mathrm{B}}_{^4\mathrm{He}}\right)_{\mathrm{gs}} = 3\hbar\omega - 6V_0 \tag{27}$$

$$\left(E^{\mathrm{B}}_{^6\mathrm{He}}\right)_{gs} = \frac{9}{2}\hbar\omega - 9V_0 \tag{28}$$

$$\left(E^{\mathrm{B}}_{^{16}O}\right)_{gs} = 12\hbar\omega - 24V_0 \tag{29}$$

$$\left(E^{\mathrm{B}}_{^{40}Ca}\right)_{gs} = 30\,\hbar\omega - 60V_0 \tag{30}$$

The potential depth for bosonic oscillators, calculated from the ground state energy which must equal the binding energy as follows:

$$(V_0)^B_{^4He} = \frac{\hbar\omega + 9.4309}{2} \tag{31}$$

$$(V_0)^B_{^6He} = \frac{1}{2}\hbar\omega + \frac{29.271}{9} \tag{32}$$

$$(V_0)^B_{^{16}O} = \frac{\hbar\omega + 10.635}{2} \tag{33}$$

$$(V_0)^B_{^{40}Ca} = \frac{\hbar\omega + 11.40174}{2} \tag{34}$$

IV. RESULTS AND DISCUSSION

In this section, we presents the results of our calculations for the thermal properties of ^{4}He, ^{6}He, ^{16}O and ^{40}Ca.We compared ^{4}He level densities with experimental data and other well-established calculations of the SMSPS [16] and the ab initio MFD [8], while only using experimental data for ^{6}He, ^{16}O and ^{40}Ca. Other results we seek in this paper is to obtain the oscillator potential depth V_0, which plays an important rule in mean field and MFD calculations.

A. Thermal properties of ^{4}He

Fig. (1) shows the level densities of ^{4}He as a function of excitation energy, calculated using 3D-SHO potential for three different values of $\hbar\omega$ as outlined in Table (1). The calculated level densities are compared with those measured experimentally, and those calculated using SMSPS method [16] and MFD ab initio technique [8]. The figure shows that the level density calculated via 3D-SHO with $\hbar\omega = 18.427$ MeV ref. [14] agrees very well with the experimental and MFD level densities.

Table 1: The adopted values of $\hbar\omega$ and references obtained from.

Ref.	$\hbar\omega(MeV)$
Shehadeh [3]	12.1482
Blomqvist and Molinar [14]	18.427
Ring and Schuck [15]	25.8284

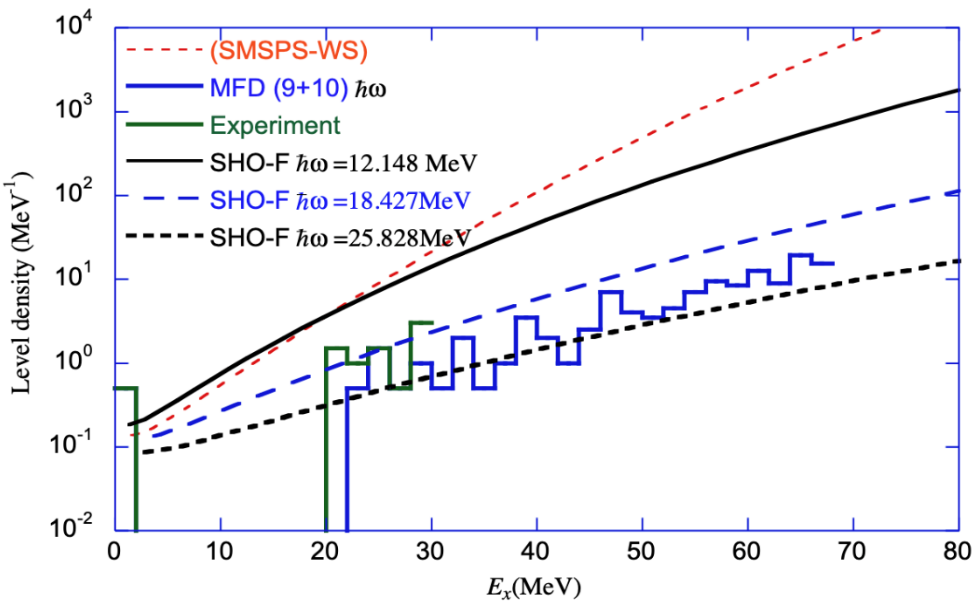

Figure 1: The level densities of ^{4}He as a function of the excitation energy, calculated using fermion gas in 3D-SHO potential at various values of $\hbar\omega$ (see legends). The results are compared with level densities calculated using SMSPS and MFD models. The experimental data histogram is obtained from counting the number of levels per unit energy per degeneracy.

Fig. (2) shows the level densities of boson gas computed at $\hbar\omega$ values range from 10 - 11 MeV, compared with those of ^{4}He fermion gas calculated using 3D-SHO at $\hbar\omega =$ 18.427 MeV, MFD ab initio, and experimental level densities. The agreement between the boson gas level density and MFD is excellent. Knowing that MFD is calculated in the following model spaces: 9 $\hbar\omega$ odd parity + 10 $\hbar\omega$ even parity states We thus conclude that the ^{4}He boson gas successfully simulates the level densities of ^{4}He.

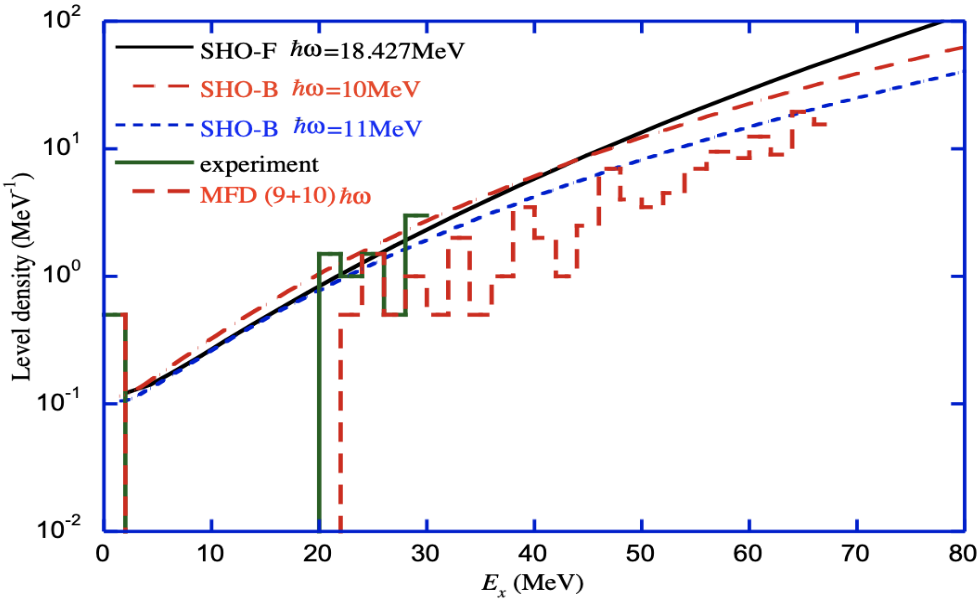

Figure 2: The level densities of ^{4}He as a function of excitation energy, calculated using boson gas in 3D-SHO potential at $\hbar\omega = 10$ and 11 MeV (see legends). The results are compared with the level densities of MFD model and the experimental data.

Fig. (3) shows the heat capacity curves in unit of Boltzmann constant k_B for various values of $\hbar\omega$ given in table (1). The heat capacities exhibit similar behaviors with different responses. It is easier to increase the internal energy of system with smaller $\hbar\omega$ as the temperature rises. This is because the energy spacings of the levels are smaller and the excitations become easier. Consequently, the heat capacity curve with the smallest $\hbar\omega$ shows the fastest rise among the three curves. All curves ultimately converge to the classical limit $3A = 12$ at higher temperature. Again, the curve with smaller $\hbar\omega$ has the fastest convergence rate, while the one with the larger $\hbar\omega$ has the slowest convergence rate. There is no indication of any quantum phase transition except for the transition from quantum to classical limit. To view how the fermion and boson gas models differ from each other for ^{4}He, we compare the heat capacities computed at the values of $\hbar\omega$ that give reliable level densities. This is shown in fig. (4). For fermion gas model we use $\hbar\omega = 18.427$ MeV and for boson gas model we use $\hbar\omega = 11$ MeV. The behavior for the two curves is quite different and we can notice a small peak near $T = 7.0$ MeV before the gas converges to the classical value of $\frac{3}{2}A = 6$. This can be a sign of phase transition in the nuclear matter, especially if we understand that this temperature is close to the binding energy per nucleon for ^{4}He. The result is very encouraging as it shows the boson gas model is more realistic than the fermion gas model to describe a highly correlated system like nuclear matter.

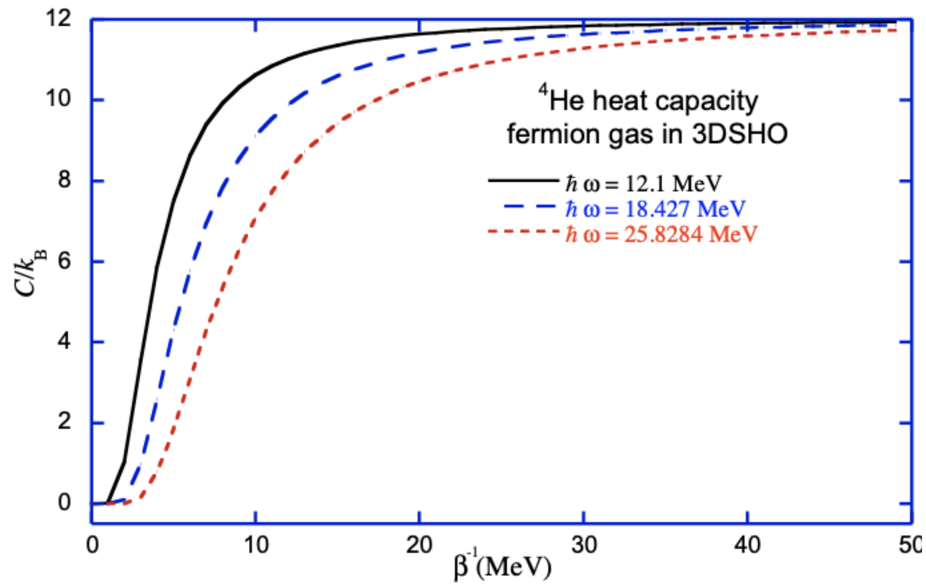

Figure 3: The heat capacities of ^{4}He at various values of $\hbar\omega$ (see legends) calculated using fermion gas model in 3DSHO.

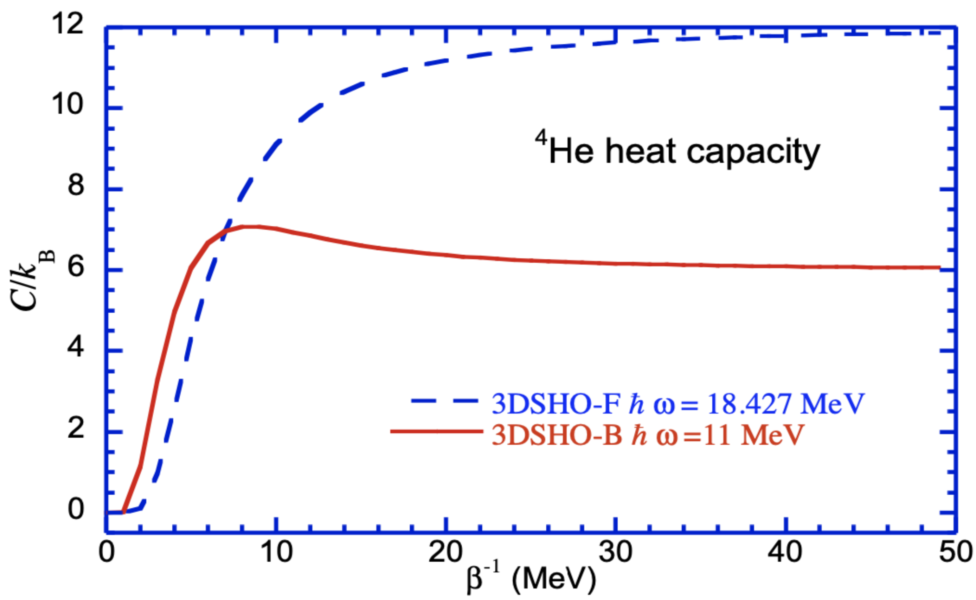

Figure 4: The heat capacities of ^{4}He calculated by two models (see legends), fermion gas model in 3DSHO at $\hbar\omega = 18.427$ MeV, and boson gas model in 3DSHO at $\hbar\omega = 11$ MeV.

level density curves of ^{4}He using various models as a function of the excitation energies are shown in fig.(5). The level density of the boson-model at $\hbar\omega = 9.2$ MeV astonishingly agrees with the experimental data. A novel technique to simulate the level density of doubly magic nuclei could extend to include all even-even nuclei.

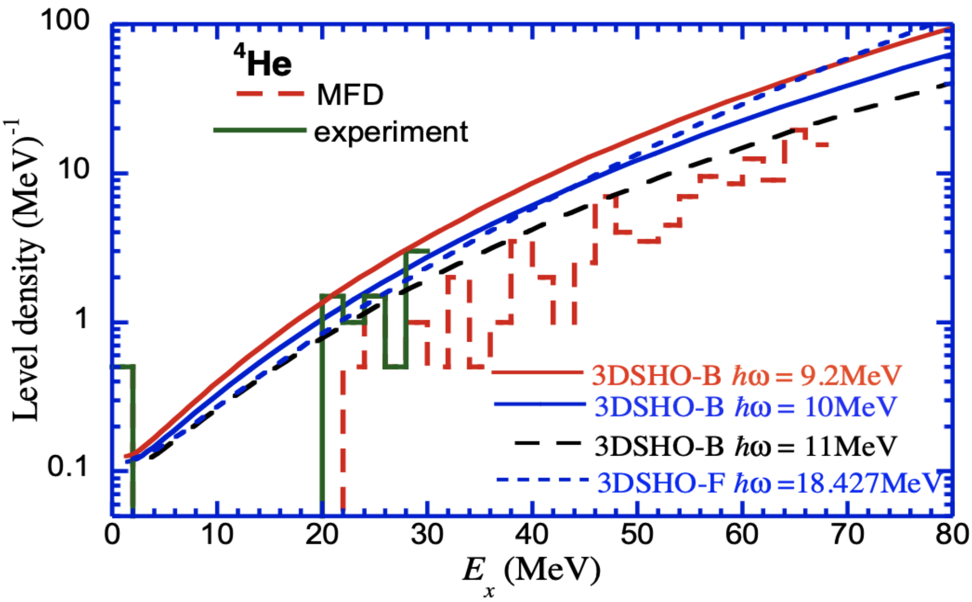

Figure 5: The level densities of ^{4}He as a function of excitation energy. The level densities are calculated using boson-gas model in 3D-SHO potential at $\hbar\omega = 9.2, 10, 11$ MeV MeV (see legends) and fermion-gas model at $\hbar\omega = 18.427$ MeV. The results are compared with level densities of MFD model and experimental data.

B. Thermal properties of ^{6}He

Table 2: The adopted values of $\hbar\omega$ and references obtained from.

Ref.	$\hbar\omega(MeV)$
Shehadeh [3]	6.6014
Blomqvist and Molinar [14]	17.1931
Ring and Schuck [15]	22.56324

Fig. (6) again confirms that the value of $\hbar\omega$ obtained from ref. [14] gives more reliable results for level density. This is clear due to the agreement with experimental data at low laying levels. For higher excitations, the experimental data fall behind the theoretical predictions. The lack of experimental results is attributed to the limitations of the energy and time resolutions of the detectors. Fig. (7) shows the heat capacity curves in unit of Boltzmann constant k_B for various values of $\hbar\omega$ given in table (2). The general behavior is similar to what we have for ^{4}He in fig. (3). The heat capacities have exactly similar behaviors with different responses. It is easier to raise the internal energy of system with smaller $\hbar\omega$ with increasing the temperature.

The effect of energy level spacings, represented by the value $\hbar\omega$ plays important role in the change of energy with temperature. All curves ultimately converge to the classical limit $3A = 18$ value at higher temperature. Again, the curve with smaller $\hbar\omega$ has the fastest convergence rate, whereas the one with the larger $\hbar\omega$ has the slowest convergence rate. There is no sign for any quantum phase transition except for the transition from quantum to classical limit.

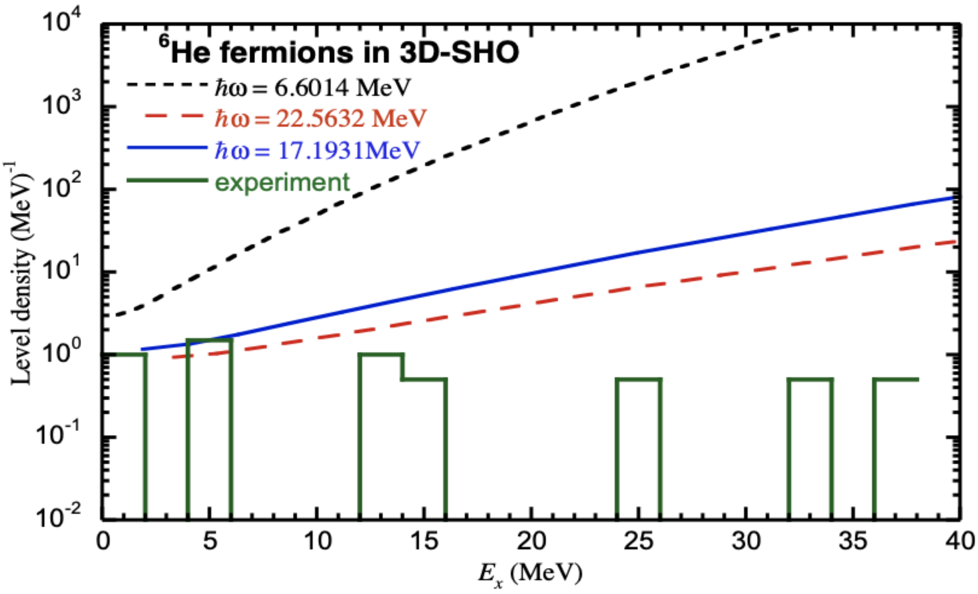

Figure 6: The level densities of ^{6}He as a function of excitation energy, calculated using fermion gas in 3D-SHO potential at various values $\hbar\omega$ (see legends). The results are compared with the experimental data.

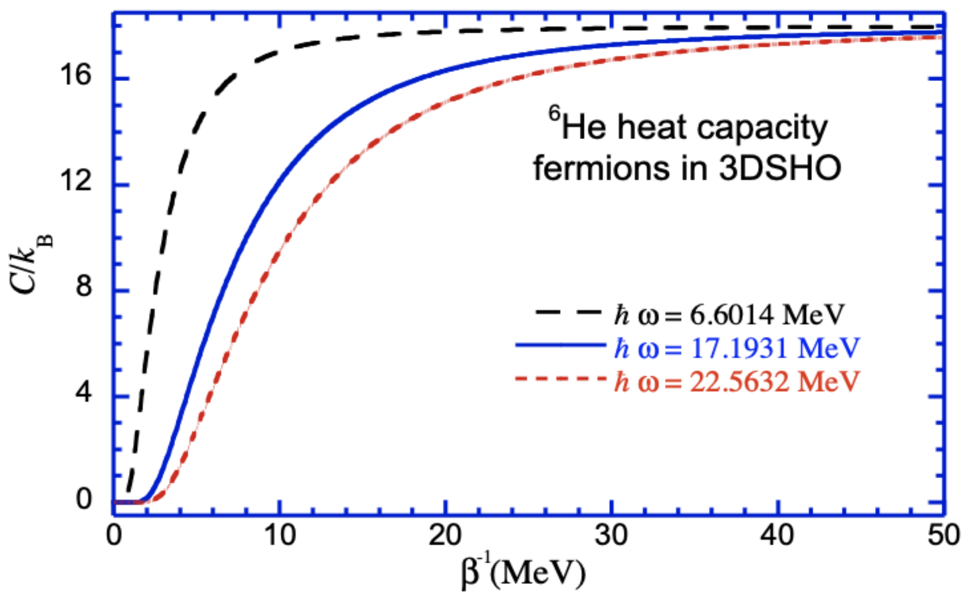

Figure 7: The heat capacity of ^{6}He at various values of $\hbar\omega$ (see legends) calculated using fermion gas in 3DSHO.

To confirm our argument, we extend this work to include two doubly magic nuclei, namely ^{16}O and ^{40}Ca.

C. Thermal properties of ^{16}O

Fig. (8) shows the level densities of ^{16}O as a function of excitation energy, calculated using fermion gas in 3DSHO potential for three different values of $\hbar\omega$ These values are given in table (3). In our initial tests with ^{16}O using the fermionic model, the $\hbar\omega$ values from table (3) did not align well with the experimental data. Consequently, we experimented with other values and determined that $\hbar\omega = 12$ MeV agrees very well with the experimental level densities.

Table 3: The adopted values of $\hbar\omega$ and references obtained from.

Ref.	$\hbar\omega(MeV)$
Shehadeh [3]	9.64205
Blomqvist and Molinar [14]	13.921
Ring and Schuck [15]	16.2708

Fig. (9) illustrates the level densities of ^{16}O as a function of excitation energy, calculated using boson gas in 3DSHO potential for three different values of $\hbar\omega$. The results indicate level density calculated with $\hbar\omega = 4.875$ MeV is in excellent agreement with the experimental data.

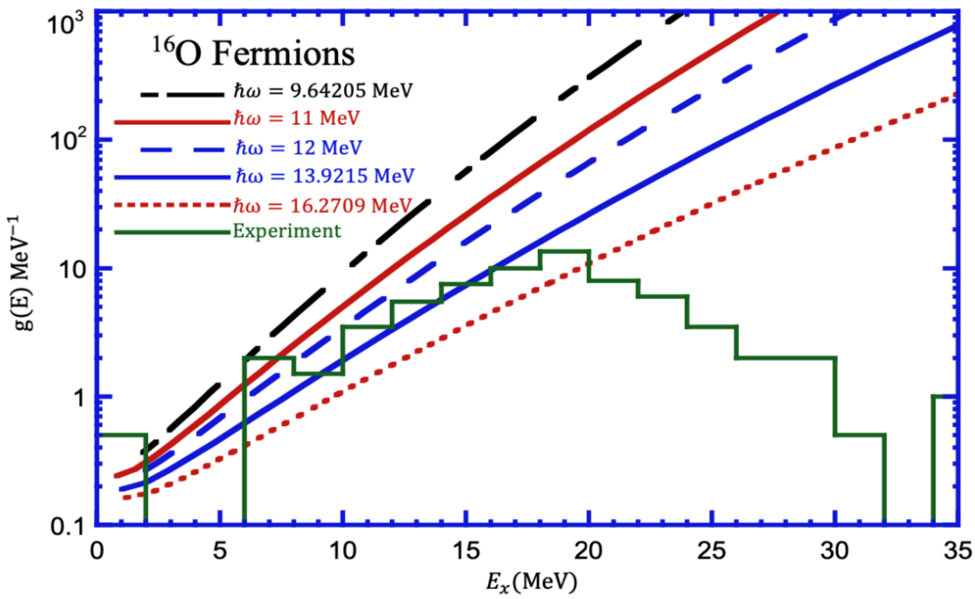

Figure 8: The level densities of ^{16}O as a function of excitation energy, calculated using 3D-SHO models for fermion gas at $\hbar\omega$ = 9.64205 MeV (black line), $\hbar\omega$ = 11 MeV (red solied line), $\hbar\omega$ = 12 MeV (blue dashed line), $\hbar\omega$ = 13.921 MeV (blue solid line) and $\hbar\omega$ = 16.2708 MeV (red dashed line). These are compared with experimental data (green stepwise).

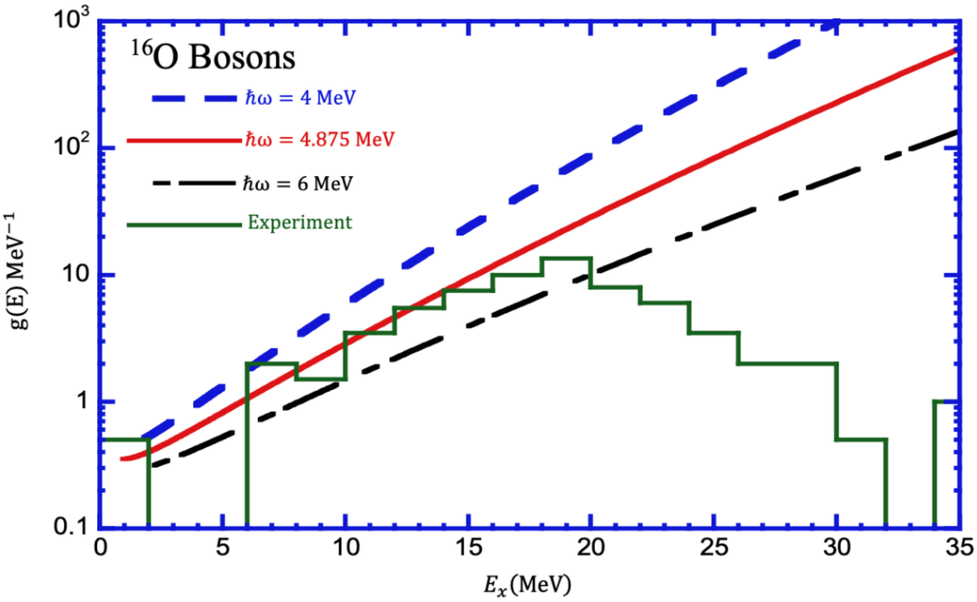

Fig.9: the level densities of ^{16}O are plotted as a function of excitation energy. Calculated using 3D-SHO models for bosons gas (blue line, $\hbar\omega$ = 4 MeV) ,(red line, $\hbar\omega$ = 4.875 MeV) and (black line, $\hbar\omega$ = 6 MeV) are compared with experimental data (green stepwise).

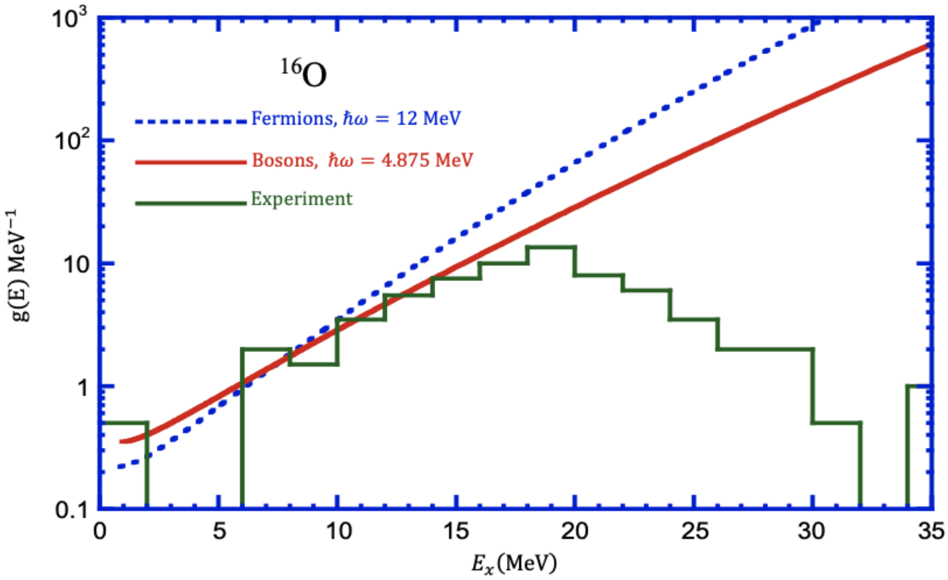

Figure 10: the level densities of ^{16}O are plotted as a function of excitation energy. Calculated using 3D-SHO models for fermion gas (blue line, $\hbar\omega$ = 12 MeV) and boson gas (red line, $\hbar\omega$ = 4.875 MeV), are compared with experimental data (green stepwise).

Fig. (11) shows the heat capacity curves in unit of Boltzmann constant k_B for various values of $\hbar\omega$ given in table (3) and $\hbar\omega = 12$ MeV. The heat capacities have exactly behaviors with different responses. It is easier to raise the internal energy of system with smaller $\hbar\omega$ with increasing the temperature. the effect of energy level spacings, represented by the value $\hbar\omega$ plays important role in the change of energy with temperature. This is why the heat capacity curve with small $\hbar\omega$ has the fastest rise among the three curves. All curves ultimately converge to the classical limit $3A = 48$ value at higher temperature. Again, the curve with smaller $\hbar\omega$ has the fastest convergence rate, whereas the one with the larger $\hbar\omega$ has the slowest convergence rate. There is no sign for any quantum phase transition except for the transition from quantum to classical limit. In Fig. (11) we notice the kink at around 4 MeV, which indicates a change in the contributions to the heat capacity**.** At lower temperatures (below this kink), the contribution to the heat capacity comes from the valence shell. At higher temperatures (above the kink), the contribution to internal energy comes from the deeper shells. To view how fermion and boson gas models differ from each other for ^{16}O, we compare the heat capacities computed at the values of $\hbar\omega$ that give reliable level densities. This is shown in fig. (12). For fermion gas model we use $\hbar\omega = 12$ MeV and for boson gas model we use $\hbar\omega$ = 4.875 MeV. The behavior for the two curves is quite different and we can notice a small peak near T = 7 MeV. Before the gas converges to the classical value of $3N = 24$, since we have 8 boson system. This could indicate a phase transition in nuclear matter, particularly considering that this temperature is close to the binding energy per nucleon for ^{16}O.

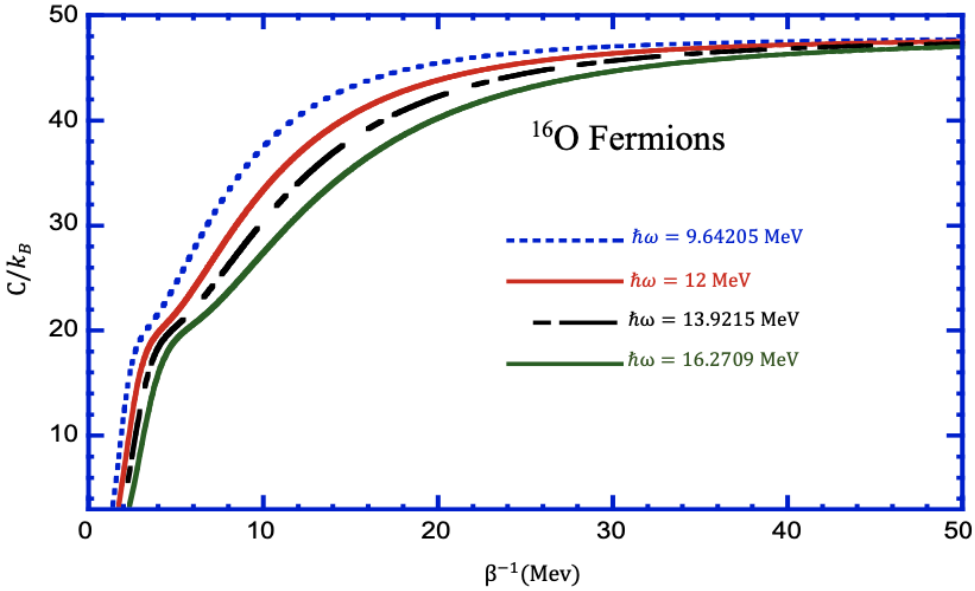

Fig.11: The heat capacity of ^{16}O as a function of inverse temperature (β^{-1}), calculated using a 3D-SHO fermion gas model at various $\hbar\omega$ values.

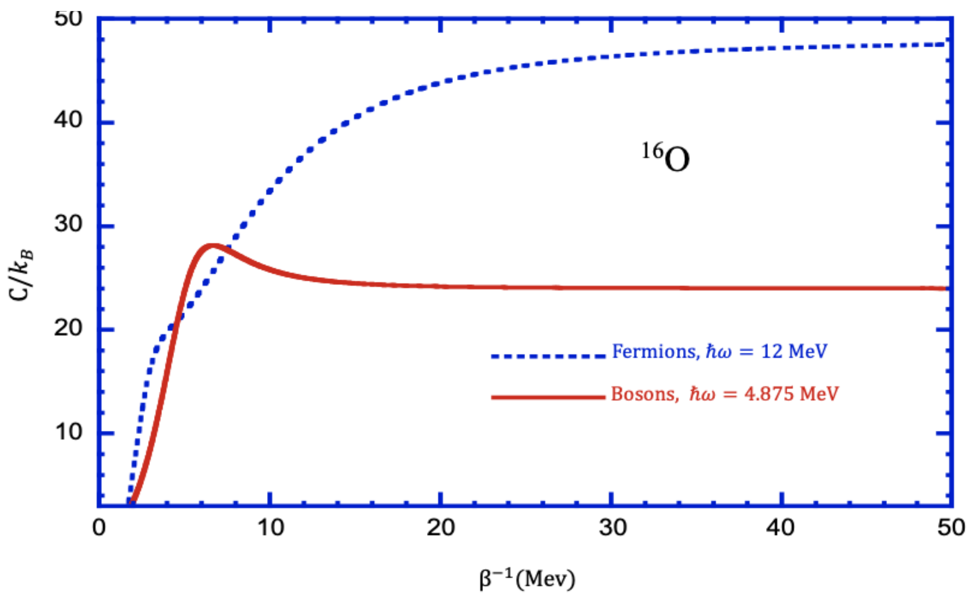

Fig.12: The heat capacity of ^{16}O as a function of inverse temperature (β^{-1}), calculated using a 3D-SHO models for fermion gas(blue line , $\hbar\omega$ = 12 MeV) and boson gas (red line, $\hbar\omega$ = 4.875 MeV).

D. Thermal properties of ^{40}Ca

Figure (13) shows the level densities of ^{40} Ca as a function of excitation energy, calculated using fermion gas in 3DSHO potential for three different values of $\hbar\omega$. These values are given in table (4). In our initial tests with ^{40} Ca using the fermionic model, the $\hbar\omega$ values from table (4) did not align well with the experimental data. Consequently, we experimented with other values and determined that $\hbar\omega = 8$ MeV agrees very well with the experimental level densities.

Table 4: The adopted values of $\hbar\omega$ and references obtained from.

Ref.	$\hbar\omega(MeV)$
Shehadeh [3]	5.23451
Blomqvist and Molinar [14]	11.0206
Ring and Schuck [15]	11.9884

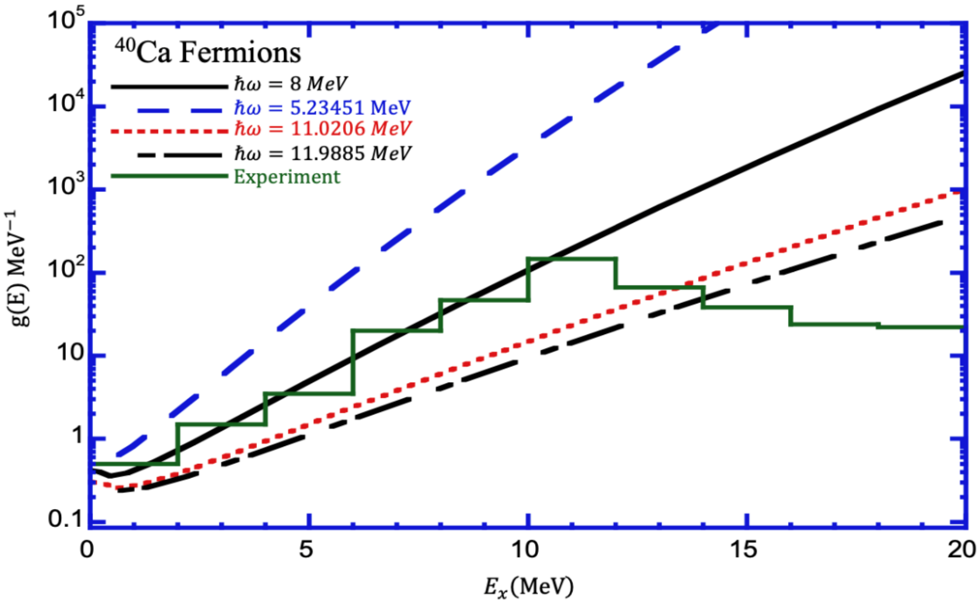

Fig.13: The level densities of ^{40} Ca as a function of excitation energy E_x, calculated using 3DSHO models for fermion gas at $\hbar\omega$ = 8 MeV (black solid line), $\hbar\omega$ = 5.23451 MeV (blue line), $\hbar\omega$ = 11.0206 MeV (red line) and $\hbar\omega$ = 11.9885 MeV (black dash-dot line). These are compared with experimental data (green stepwise).

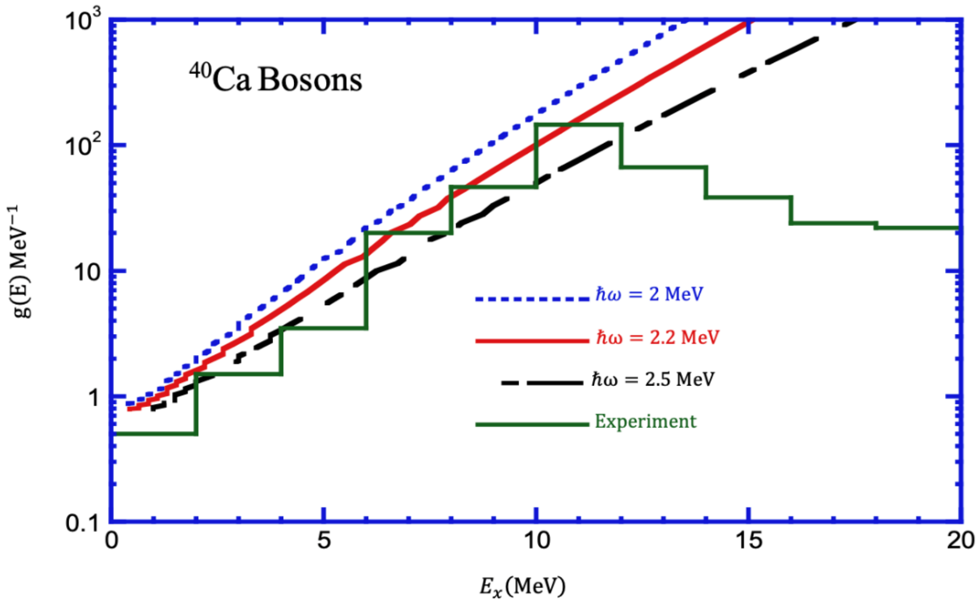

Fig.14: the level densities of ^{40} Ca are plotted as a function of excitation energy E_x. Calculated using 3DSHO models for boson gas (blue dashed line, $\hbar\omega$ = 2 MeV), (red line, $\hbar\omega$ = 2.2 MeV) and (black line, $\hbar\omega$ = 2.5 MeV), are compared with experimental data (green stepwise).

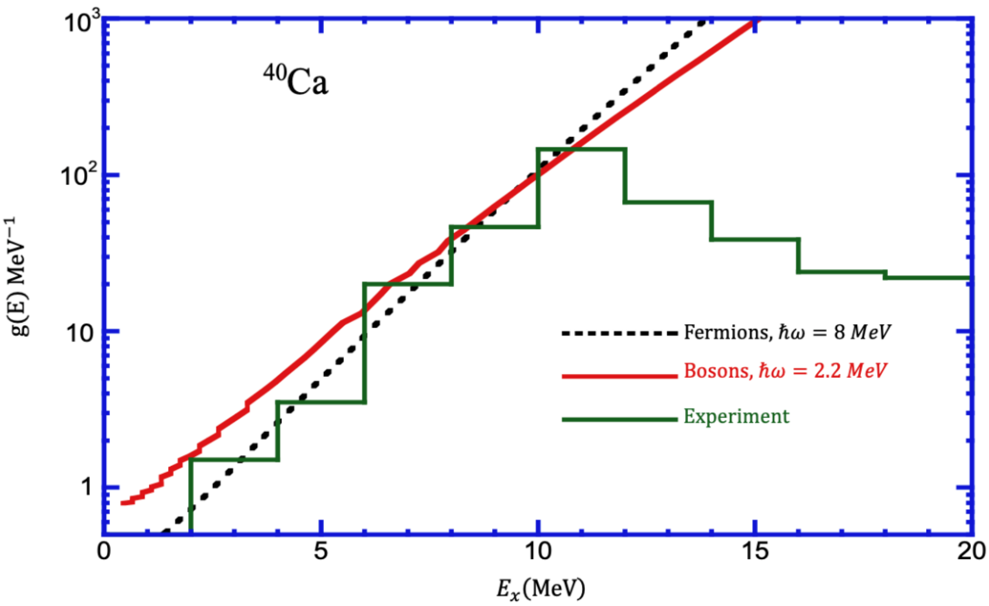

Fig.15: the level densities of ^{40} Ca are plotted as a function of excitation energy E_x. Calculated using 3DSHO models for fermion gas (black line, $\hbar\omega$ = 8 MeV) and boson gas (red line, $\hbar\omega$ = 2.2MeV), are compared with experimental data (green stepwise).

Fig. (14) illustrates the level densities of ^{40} Ca as a function of excitation energy, calculated using boson gas in 3DSHO potential for three different values of $\hbar\omega$. The results indicate level density calculated with $\hbar\omega = 2.2\ MeV$ is in excellent agreement with the experimental data. Fig. (16) shows the heat capacity curves in unit of Boltzmann constant k_B for various values of $\hbar\omega$ given in table (4) and $\hbar\omega = 8$ MeV . The heat capacities have exactly behaviors with different responses. It is easier to raise the internal energy of system with smaller $\hbar\omega$ with increasing the temperature. the effect of energy level spacings, represented by the value $\hbar\omega$ plays important role in the change of energy with temperature. This is why the heat capacity curve with small $\hbar\omega$ has the fastest rise among the three curves. All curves ultimately converge to the classical limit $3A = 120$ value at higher temperature. Again, the curve with smaller $\hbar\omega$ has the fastest convergence rate, whereas the one with the larger $\hbar\omega$ has the slowest convergence rate. There is no sign for any quantum phase transition except for the transition from quantum to classical limit. In fig. (4.16) we notice the kink at around 3 MeV, which indicates a change in the contributions to the heat capacity. At lower temperatures (below this kink), the contribution to the heat capacity comes from the valence shell. At higher temperatures (above the kink), the contribution is due to the deeper shells. To view how fermion and boson gas models differ from each other for ^{40}Ca, we compare the heat capacities computed at the values of $\hbar\omega$ that give reliable level densities. This is shown in fig. (17). For fermion gas model we use $\hbar\omega = 8$ MeV and for boson gas model we use $\hbar\omega$ = 2.2 MeV. The behavior for the two curves is quite different and we can notice a small peak near $T = 4$ MeV. Before the gas converges to the classical value of $3N = 60$, since we have 20 boson system. This could indicate a phase transition in nuclear matter, particularly considering that this temperature is close to the binding energy per nucleon for ^{16}O.

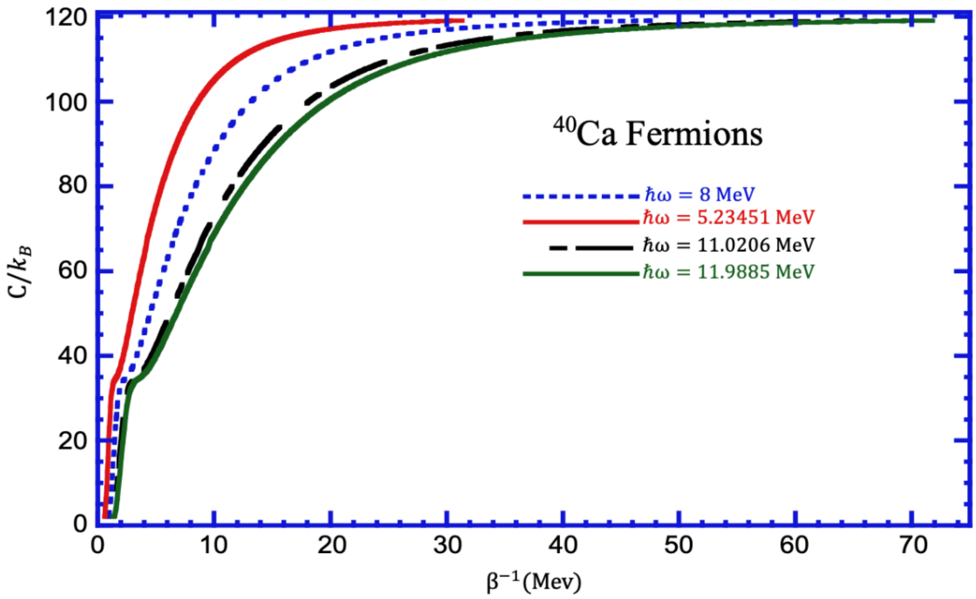

Fig.16: The heat capacity of ^{40}Ca as a function of inverse temperature (β^{-1}), calculated using a 3D-SHO fermion gas model at various $\hbar\omega$ values.

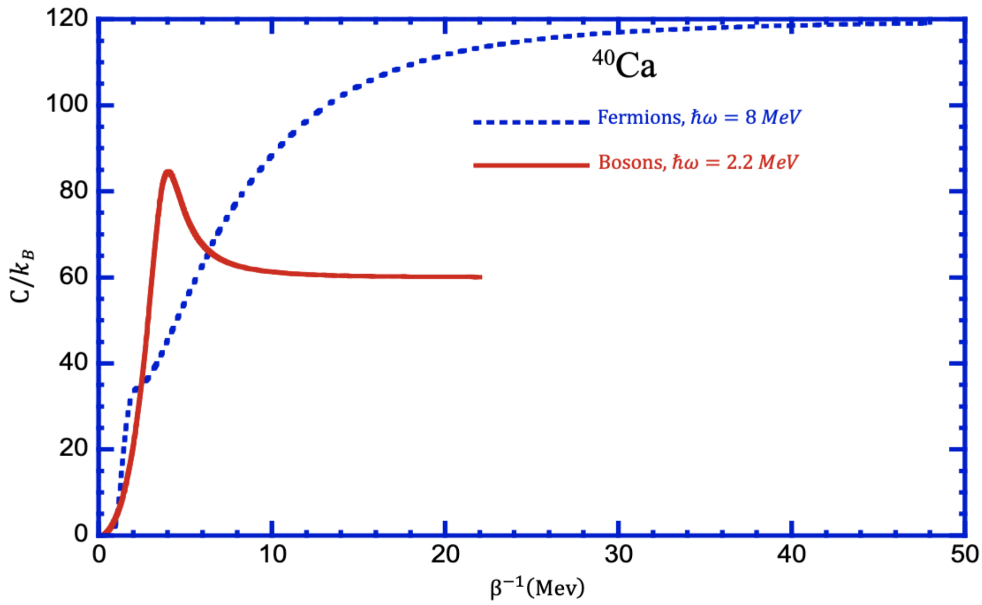

Fig.17: The heat capacity of ^{40}Ca as a function of inverse temperature (β^{-1}), calculated using a 3D-SHO models for fermion gas(blue line , $\hbar\omega = 8$MeV) and boson gas (red line, $\hbar\omega = 2.2$ MeV).

E. Potential depth

Phenomenological potential depth plays important role in generating the quantum states for the bound systems. The initial correct value speeds up the convergence process of state generation using the Hartree-Fock method or matrix diagonalization in multi-fermion dynamics code [8]. It is an advantage to use the ground state energy to predict the values of the potential depths and compare it with the experimental values of the binding energies.

Table (5) summarizes the oscillator's potential depth V_0 for ^{4}He, ^{6}He, ^{16}O and ^{40}Ca, as calculated within the 3DSHO model for fermions. Table (6) outlines the potential depth V_0 for bosons, reflecting different modeling requirements and implications in the behavior of fermions versus bosons under similar conditions.

Table 5: potential depth (V_0) for fermions: ^{4}He, ^{6}He, ^{16}O and ^{40}Ca

3DSHO Model fermions	$\hbar\omega$(MeV)	Potential depth V_0(MeV)	BE(MeV)	BE/A(MeV)
^{4}He	18.43	11.57	-28.30	-7.07
^{6}He	17.19	12.13	-29.27	-4.88
^{16}O	12	11.65	-127.6193	-7.9762
^{40}Ca	8	10.85	-342.0522	-8.5513

Table 6: potential depth (V_0)for bosons: ^{4}He, ^{6}He, ^{16}O and ^{40}Ca

3DSHO Model bosons	$\hbar\omega$(MeV)	Potential depth V_0(MeV)	BE(MeV)	BE/A(MeV)
^{4}He	9.20	9.31	-28.30	-7.07
^{6}He	3.73	5.12	-29.27	-4.88
^{16}O	4.87	7.75	-127.6193	-7.9762
^{40}Ca	2.2	6.8	-342.0522	-8.5513

In conclusion, using an appropriate mean-field potential within the 3DSHO treatment yields a successful model. approximately predicting the level densities for ^{4}He, ^{16}O and ^{40}Ca, which align well with experimental data. This success in describing the level densities lends significant support to the model's predictions. The prediction power of the model is drastically improved if one can correctly calculate the values of $\hbar\omega$ for relevant nuclei. We can execute such calculation by fitting the optimal $\hbar\omega$ values versus A for doubly magic nuclei. In fig. (18). shows best fitting of $\hbar\omega$ using the function, we know

$$\hbar\omega = CA^{-\alpha}.$$

For fermions, the best fit is

$$\hbar\omega = 30.5358A^{-0.35492} \text{ MeV}, \tag{35}$$

and for Bosons,

$$\hbar\omega = 30.5358A^{-0.60823} \text{ MeV}. \tag{36}$$

The fitting shown in fig. (19). applies solely to the nuclei ^{4}He, ^{16}O and ^{40}Ca establish this fitting as definitive, further data collection is necessary. Expanding the dataset to include additional measurements from these and potentially other nuclei would provide the validation needed to generalize this model more widely.

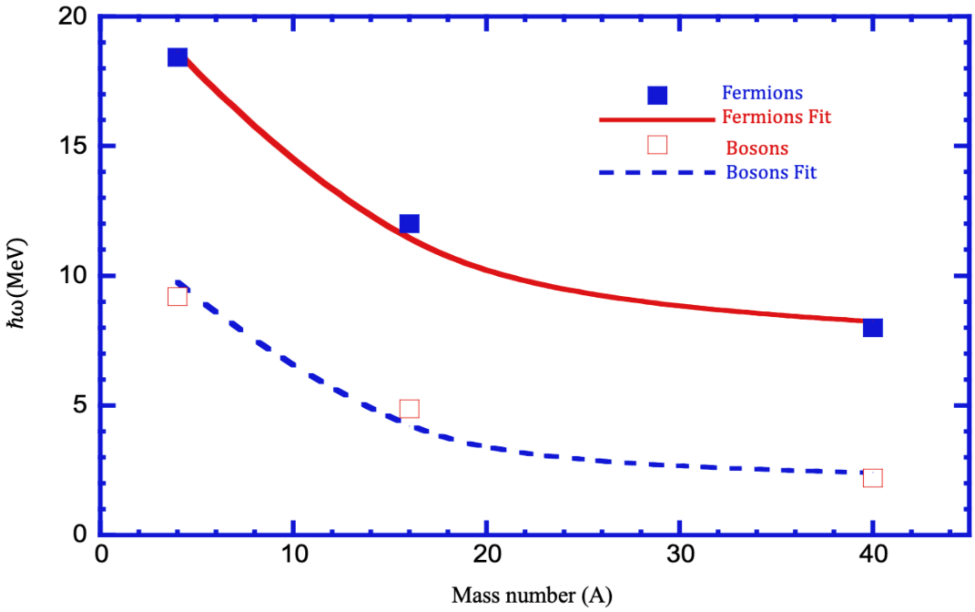

Figure 18: variation of $\hbar\omega$ values versus the mass number A for fermions and bosons (A= *4 to 40*), illustrating fitted values.

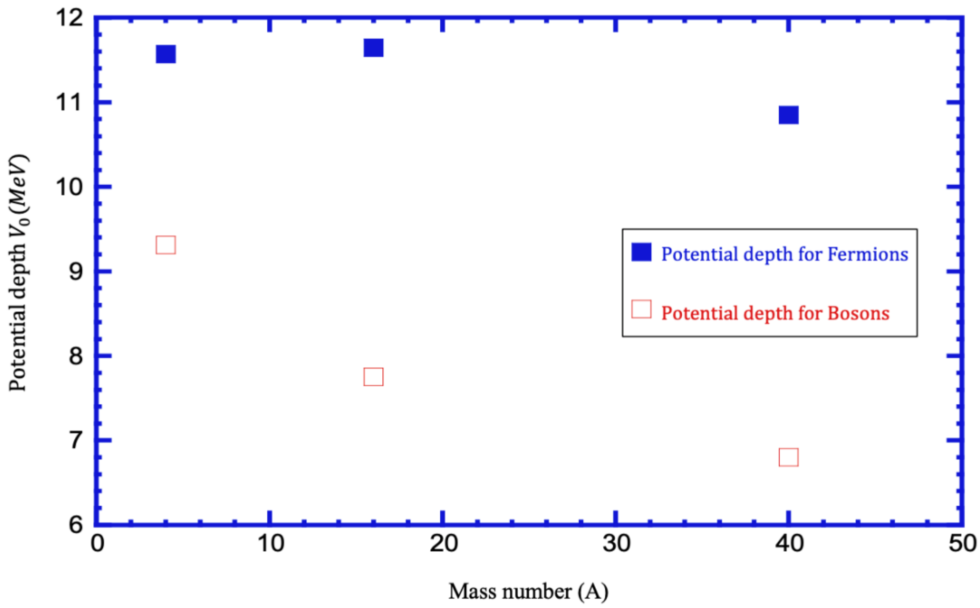

Figure 19: variation of Potential depth (V_0) versus mass number (A) for fermions and bosons. The nuclei here range from A= 4 to 40.

V. CONCLUSION AND FURTHER RESEARCH

Our study demonstrates that modeling nuclear matter for doubly magic nuclei (^{4}He, ^{16}O, and ^{40}Ca) as either Fermion or Boson gases with $\hbar\omega$ values as specified in equations (35) and (36) can accurately predict experimental level densities. This approach also enables the derivation of potential depth values presented in Tables (5) and (6), which are useful for subsequent scattering cross-section calculations. Notably, the heat capacity calculations indicate a pronounced phase transition in the nuclear matter for Boson gases at approximately 7 MeV for ^{4}He, 6 MeV for ^{16}O, and 4 MeV for ^{40}Ca. Beyond these temperatures, the nuclear matter exhibits characteristics of a classical gas.

Future research should explore open shell nuclei by considering them as comprising a core and valence nucleons. In this framework, the core is modeled as a Boson gas of isoscalar, spin-vector quasi pn-particles in a three-dimensional harmonic oscillator potential, with the valence nucleons treated as either Fermion or Boson gases, depending on the number of protons and neutrons. This approach has the potential to further refine our understanding of nuclear matter properties and phase transitions.

[1] D.Q. Lamb et al., Phys. Rev. Lett. 41, 1623 (1978).

[2] H.-J. Schmidt, and J. Schnack, Physica A, 260, 479 (1998).

[3] B.A. Shehadeh, "Statistical and thermal properties of mesoscopic systems: Application to the many-nucleon system." PhD dissertation, July 2003, Department of Physics and Astronomy, Iowa State University, Ames, Iowa.

[4] P. Borrmann, and G. Franke, J. Chem. Phys. 98, 2484 (1993).

[5] K. Chase and A. Mekjian, Phys. Rev, C49, 2164 (1994); Phys. Rev, C50, 2078 (1994).

[6] K. Chase, A. Mekjian, and L. Zamick, Europ. Phys. Journal, B8, 281 (1999).

[7] S. Pratt, Phys. Rev. Lett. 84, 4255 (2000).

[8] B. Shehadeh, J. Vary, M. Hasan, Phys. Rev. C, submitted.

[9] H.-J. Schmidt, and J. Schnack, Physica A, 265, 584 (1999).

[10] F. Brosens, L.F. Lemmens, and J.T. Deveerse, Phys. Rev. E55, 227 (1997).

[11] F. Brosens, J.T. Deveerse, and L.F. Lemmens, Phys. Rev. E57, 3871 (1998).

[12] Y. Hida, X.S. Li and D.H. Bailey, "Algorithms for Quad-Double Precision Floating Point Arithmetic.", In Proceedings of ARITH-15, IEEE Computer Society, 2001.

[13] Y. Hida, X.S. Li and D.H. Bailey, "Quad-Double Arithmetic: Algorithms, Implementation, and Application.", Technical Report LBNL-46996, Lawrence Berkeley National Laboratory, Berkeley, CA 94720, Oct. 2000.

[14] J. Blomqvist and A. Molinari. Collective 0 vibrations in even spherical nuclei with tensor forces. Nuclear Physics A, 106(3):545–569, 1968.

[15] P. Ring and P. Schuck. The Nuclear Many-Body Problem. Physics and astronomy online library. Springer, 2004.

[16] Bassam Shehadeh and James P. Vary. Statistical properties of 56-57fe with multi-shell degrees of freedom, 2018.